Applied Catalysis B: Environmental 132–133 (2013) 321–331

Contents lists available at SciVerse ScienceDirect

Applied Catalysis B: Environmental

journal homepage: www.elsevier.com/locate/apcatb

Reactive adsorption of hydrogen sulfide on visible light photoactive zinc (hydr)oxide/graphite oxide and zinc (hydr)oxychloride/graphite oxide composites

Oluwaniyi Mabayoje[a], Mykola Seredych[a], Teresa J. Bandosz[b,*]

[a] The City College of New York, Department of Chemistry, 160 Convent Avenue, New York, NY 10031, USA
[b] The City College of New York, Department of Chemistry, CUNY Energy Institute, 160 Convent Avenue, New York, NY 10031, USA

ARTICLE INFO

Article history:
Received 28 August 2012
Received in revised form 5 December 2012
Accepted 7 December 2012
Available online 20 December 2012

Keywords:
Visible light activity
Graphite oxide
Zinc (hydr)oxide
Zinc (hydr)oxychlorides
Composites
H_2S adsorption
Surface reactivity

ABSTRACT

Composites of zinc (hydr)oxide and graphite oxide (GO) with 2, 5, and 20 wt.% of the GO component were obtained by precipitating zinc hydroxide from zinc chloride with dispersed GO present in the solution. The materials were evaluated as adsorbents of hydrogen sulfide at ambient conditions. The surface properties of the initial and exhausted samples were studied by FTIR, XRD, SEM/EDX, TEM, nitrogen adsorption, potentiometric titration, microcalorimetry, and thermal analysis. The adsorption capacity increases with an increase in the content of GO in the composites studied. The lower adsorption capacities measured for the samples with 2 and 5 wt.% of graphite oxide are linked to the zinc (hydr)oxychlorides phase present in these composites. The heats of H_2S adsorption on the zinc (hydr)oxide and its composites were measured in nitrogen and in air flow. The results indicate that highly energetic adsorption centers are formed on the composite surfaces. Exposure to visible light decreases the H_2S adsorption capacity. This behavior is linked to photoactivity that leads to the reduction of the composite and formation of sulfur and sulfites/sulfates. These processes involve active centers, —OH groups, which react with hydrogen sulfide.

© 2012 Elsevier B.V. All rights reserved.

1. Introduction

Hydrogen sulfide is a toxic pollutant present in the atmosphere as a result of anaerobic bacterial reduction of sulfates. The inhalation of hydrogen sulfide can be lethal for humans as it attacks the neural system and important organs [1]. Materials that have been applied for the removal of H_2S at high temperatures include zeolites, modified alumina, or metal oxides [2,3]. Modified activated carbons are typically used at ambient conditions [4]. The modification methods focus on an increase in surface basicity to enhance H_2S dissociation. The approaches used include impregnation with caustics or alkali metal salts [5,6] and the incorporation of nitrogen functional groups [7,8]. Another group of carbonaceous materials studied as adsorbents of hydrogen sulfide are graphite oxide-based materials [7,9–11]. Although the graphite oxide's structure and chemistry depend on various factors like the level of oxidation and on the type of oxidizing agents used, it can generally be represented as distorted graphene layers decorated with different oxygen functional groups [12–15]. These oxygen groups enable GO dispersion in many solvents and they also participate in the formation of various composite materials.

Composites of graphite oxide or graphene with zinc (hydr)oxide were recently studied as adsorbents of H_2S at ambient conditions [9]. The results showed that an addition of graphite oxide or graphene significantly improves the performance of these materials, especially in moist conditions. The conversion of H_2S to SO_2 on the surface was enhanced by photocatalytic activity in visible light. The synergistic effect of the GO component was linked to the structure of the composite where the zinc (hydr)oxide component had more terminal groups than its bulk phase. These groups were shown to take part in oxidation reactions via a photochemical path. The graphite oxide and graphene components also helped in electron transfer leading to oxygen activation. The better adsorption capacity on the GO composites than that on $Zn(OH)_2$ was linked to more terminal OH groups, to the presence of oxygen activating functional groups and to bonds between zinc (hydr)oxide and the graphene oxide in the composites. Products formed on the surface after H_2S adsorption included elemental sulfur, sulfite, sulfate species and zinc sulfide.

The synergistic effect on the surface of cobalt (hydr)oxide/GO composites was also shown to be important for the reactive adsorption of H_2S, especially in moist conditions [10]. The adsorption process was significantly enhanced when a small amount of

* Corresponding author. Tel.: +1 212 650 6017; fax: +1 212 650 6107.
E-mail address: tbandosz@ccny.cuny.edu (T.J. Bandosz).

0926-3373/$ – see front matter © 2012 Elsevier B.V. All rights reserved.
http://dx.doi.org/10.1016/j.apcatb.2012.12.011

graphite oxide was present in the composite. The new chemical environment at the interface was shown to contribute to the extent of H_2S dissociation. Superoxide ions formed as a result of the incorporation of heteroatoms into the graphene oxide matrix were indicated as important participants in H_2S oxidation reactions. A high adsorption capacity on the composites with the low ratio of GO was explained taking into account a unique structure and chemistry of the composites. The presence of a small amount of highly dispersed graphite oxide sheets resulted in a very amorphous and chemically heterogeneous material with a significant number of oxygen vacancies and terminal hydroxyl groups. These sites helped in the oxidation and reactive adsorption. The presence of cobalt in lower oxidation states in the materials with a higher carbonaceous component content, which was a result of the reducing effect of graphene layers on metal oxide nanoparticles, had a negative effect on the adsorption of H_2S.

This paper aims to further investigate the interactions of zinc (hydr)oxide/GO composites with hydrogen sulfide. Various contents of GO were chosen to evaluate the effect of the amount of GO on the materials' chemical and physical properties and on their performance as hydrogen sulfide adsorbents. The results obtained in ambient light and in dark are expected to shed a new light on photoactivity of the zinc (hydr)oxide/GO composites. This photoactivity might be an important factor for applications of these materials as reactive adsorbents and catalysts [16–18].

2. Experimental

2.1. Materials preparation

Graphite oxide was synthesized by oxidation of graphite (Sigma–Aldrich) using the Hummers method [19]. Graphite powder (10 g) was stirred with cool concentrated sulfuric acid (230 mL at 0 °C). Then, potassium permanganate (30 g) was added slowly to the suspension to prevent a rapid rise in the temperature (less than 20 °C). The reaction mixture was then cooled to 2 °C. After removal of the ice-bath, the mixture was stirred at room temperature for 30 min. Distilled water (230 mL) was slowly added to the reaction vessel to keep the temperature under 98 °C. The diluted suspension was stirred for an additional 15 min and further diluted with distilled water (1.4 L), before adding hydrogen peroxide (100 mL). The mixture was left overnight. GO particles, settled at the bottom, were separated from the excess liquid by decantation followed by centrifugation. The remaining suspension was transferred to dialysis tubes (MW cutoff 6000–9000). Dialysis was carried out until no precipitate of $BaSO_4$ was detected by addition of $BaCl_2$. Then, the wet form of graphite oxide was centrifuged and freeze-dried. A fine brown powder of the initial graphite oxide was obtained. The resulting material is referred to as GO.

The composite material GO/zinc (hydr)oxide was prepared by dispersing GO powder (2, 5 and 20 wt.% of the final mass of the material) in 1.0 L of zinc chloride (0.05 M). The resulting well-dispersed suspension was stirred for 4 h. A sodium hydroxide solution (0.05 M) was then added (2.0 L) to the dispersed graphene-base phases with a rate 2.0 mL/min using a Titronic Universal (SCHOTT). Then, the obtained composites were extensively washed with distilled water until neutral pH and no traces of chlorine ion were found in the leachates. Finally, the suspension was centrifuged and the gel formed was dried at 100 °C for 2 days. The composites are referred to as ZnGO-2, ZnGO-5 and ZnGO-20. The numbers represent the weight percent of graphite oxide in the composites.

The samples after exposure to H_2S in moist conditions have the suffix E added to their name. Letter L refers to the experiments run in ambient light and D- to those run in dark conditions.

2.2. Characterization of materials

2.2.1. FTIR spectroscopy

Fourier transform infrared (FTIR) spectroscopy was carried out using a Nicolet Magna-IR 830 spectrometer using the attenuated total reflectance (ATR) method. The spectrum was generated and collected 32 times and corrected for the background noise. The experiments were done on the powdered samples, without KBr addition.

2.2.2. Thermal analysis

Thermogravimetric (TG) curves were obtained using a TA instrument thermal analyzer. The initial and exhausted samples were exposed to an increase in temperature (10 °C/min) while the nitrogen flow rate was held constant (100 mL/min). From the TG curves, differential TG (DTG) curves were derived.

2.2.3. pH of the surface

A 0.1 g sample of dry adsorbent was added to 5 mL of deionized water and the suspension stirred overnight to reach equilibrium. The pH of suspension was measured using an Accumet Basic pH meter (Fisher Scientific, Springfield, NJ, USA).

2.2.4. Nitrogen adsorption

N_2 isotherms were measured at −196 °C using an ASAP 2020 (Micromeritics, Surface area and Porosity Analyzer Norcross, GA, USA). Prior to each measurement, initial samples were outgassed at 120 °C to vacuum 10^{-4} Torr. The surface area, S_{BET} (Brunauer–Emmet–Teller method was used), the micropore volume, V_{mic} (calculated using the Dubinin–Radushkevich approach) [20] the mesopore volume, V_{mes}, the total pore volume, V_t (calculated from the last point of the isotherms based on the volume of nitrogen adsorbed) were calculated from the isotherms. The volume of mesopores, V_{mes}, represents the difference between the total pore volume and the micropore volume.

2.2.5. Potentiometric titration

Potentiometric titration measurements were performed with a DMS Titrino 716 automatic titrator (Metrohm). Volumetric standard NaOH (0.1 M) was used as the titrant starting from the initial pH of the materials suspension up to pH 11. The experimental data was transformed into a proton binding curves, *Q*, representing the total amount of protonated sites [21,22].

2.2.6. X-ray diffraction (XRD)

XRD measurements were conducted using standard powder diffraction procedures. Adsorbents were ground with methanol in a small agate mortar. The mixture was smear-mounted and then analyzed by CuK_α radiation (tension −40 kV and current −40 mA) generated in a Phillips X'Pert X-ray diffractometer. A standard glass slide was run for the background. The diffraction patterns were collected from 5° to 70° at absolute scan.

2.2.7. SEM/EDX

Scanning electron microscopy images were obtained using a Zeiss Supra 55 VP with an accelerating voltage of 15.00 kV. Scanning was performed in situ on a powder sample. SEM images with energy-dispersive X-ray (EDX) analysis were done at 10 KX magnifications. The areas analyzed were 456 μm^2 and the difference in the atomic contents of elements on the surface between the results collected from different areas was less than 2–4%.

2.2.8. TEM

Transmission electron microscopy (TEM) was performed on a Zeiss EM 902 instrument. The microscope has a line resolution of 0.34 nm and a point resolution of 0.5 nm; operates in normal,

diffraction and low dose modes at 50 or 80 kV. Analyses were done after the samples were re-suspended in ethanol.

2.2.9. Differential scanning microcalorimetry

The heat of adsorption of zinc (hydr)oxide/graphite oxide composites was measured at 25 °C using the Calvet type DSC (calorimetric detector-3D sensor). Tight connections of silica reactive tube with known mass of sample were adjusted at both ends of the tubes for the gas inlet and outlet. Prior to the test, the sample was equilibrated in N_2 or air atmosphere with a flow 100 mL/min at constant temperature. Then the reactive gas (H_2S with a flow 25 mL/min, initial concentration 1000 ppm) was introduced at 25 °C with a continuous flow of N_2 or air. The heat of adsorption in J/g was calculated by integration of peaks corresponding to H_2S adsorption.

2.3. H_2S breakthrough dynamic test

In order to determine the breakthrough capacities of the materials studied, dynamic breakthrough tests were performed at room temperature. In a typical test [23], a flow of H_2S diluted with either dry or moist air were passed through a fixed bed (bed diameter 0.9 cm; height: ~1.5 cm; particle size: 0.4–0.6 mm) of adsorbent with a total inlet flow rate of 500 mL/min for H_2S with the initial concentration of 1000 ppm. The adsorbent's bed volume was about 1.5 cm^3. The concentration of H_2S in the outlet gas was measured using an electrochemical sensor (Multi-Gas Monitor, RAE system). The tests were arbitrary stopped at 100 ppm (sensor limits) and then the adsorption capacity of each adsorbent was calculated in mg/g of the material by integration of the area above the breakthrough curve. Before the H_2S test performed in moist air the adsorbent bed was prehumidified for 2 h by exposing it to air flow with 75% relative humidity. After the breakthrough tests, all samples were exposed to a flow of carrier air (400 mL/min) to impose the desorption of the H_2S and thus to evaluate the strength of its retention. The suffixes -D and -L are added to the name of the samples after the exposure to the gas in dark and in ambient light, respectively.

3. Results and discussion

3.1. Characterization of materials

The X-ray diffraction patterns for the materials studied are presented in Fig. 1. Visible differences are a clear indication of the variations not only in the level of crystallinity but also in surface chemistry. Apparently ZnGO-2 lacks a crystalline phase of $ZnO/Zn(OH)_2$. This phase is visible in ZnGO-5 and ZnGO-20. The positions of the diffraction peaks at 11.52°, 19.95°, 20.75°, 28.51°, 32.74° and 36.02° suggest that zinc (hydr)oxychloride, $Zn_5(OH)_8Cl_2{\cdot}nH_2O$, is present in ZnGO-2 and ZnGO-5 as a crystalline phase [24]. This suggests that a "fraction" of —OH groups from graphite oxide is involved in the formation of new species in the composites. Thus the samples with small amounts of GO retains the zinc (hydr)oxychlorides crystallographic phase while the sample with highest amount of GO exhibits the characteristic peaks for $ZnO/Zn(OH)_2$ at 31.74°, 34.37°, 36.32°, 56.67°, 62.60° and 68.22° [25]. The —COOH groups on the edge of GO also participate in the formation of composite as seen in the case of ZnGO-20 with the pattern of zinc hydr(oxy)acetate, $Zn(OH)_{1.58}(CH_3COO)_{0.42}{\cdot}0.31H_2O$ [26]. The peak at 2θ 10.27° for GO indicates that the material has a well formed layered structure with a d_{002} 7.60 Å. Those differences in the chemistry and structure are expected to contribute to the differences in the adsorption capacity. Even though the inorganic phase should be predominant in ZnGO-2, its totally different chemistry than that of $Zn(OH)_2$ and replacement of —OH groups

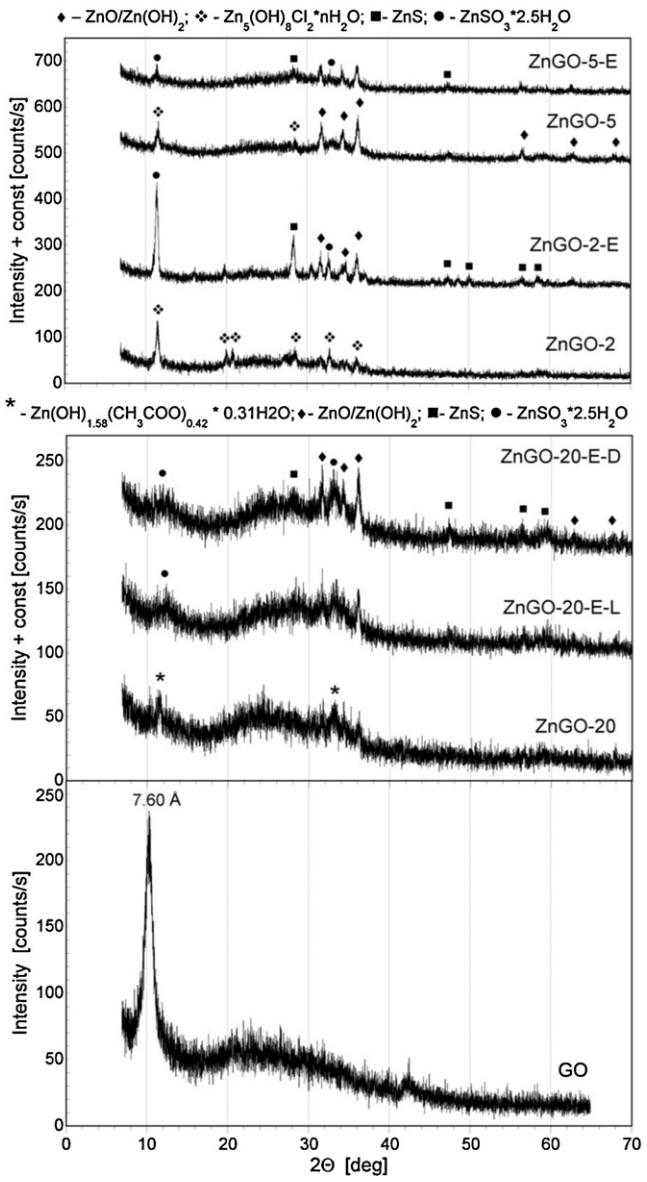

Fig. 1. XRD patterns for the initial and exhausted materials.

with Cl ions may affect the number of reactive adsorption sites for H_2S [9].

The X-ray diffraction results are supported by EDX analysis of the composite surfaces. The contents of elements on the surface in an atomic percent are collected in Table 1 and the maps of the elements are presented in Fig. 2. In both ZnGO-2 and ZnGO-5 chloride was detected and in the former sample the amount of Cl is six times higher than that in the latter one. The content of carbon increases with an increase in the content of the GO phase but apparently the distribution of this phase differs between the samples and ZnGO-5 has a relatively high amount of carbon on the surface. Interesting conclusion can be drawn from the analysis of the zinc to oxygen

Table 1
Content of elements (C, O, Cl, Zn, S) in atomic percent in the materials studied.

Sample	C (at.%)	O (at.%)	Cl (at.%)	Zn (at.%)	S (at.%)
ZnGO-2	13.6	24.2	8.2	54.0	–
ZnGO-5	33.9	32.0	1.4	32.7	–
ZnGO-20	55.9	29.3	–	14.8	–
ZnGO-20-E-L	49.9	15.6	–	27.8	6.7

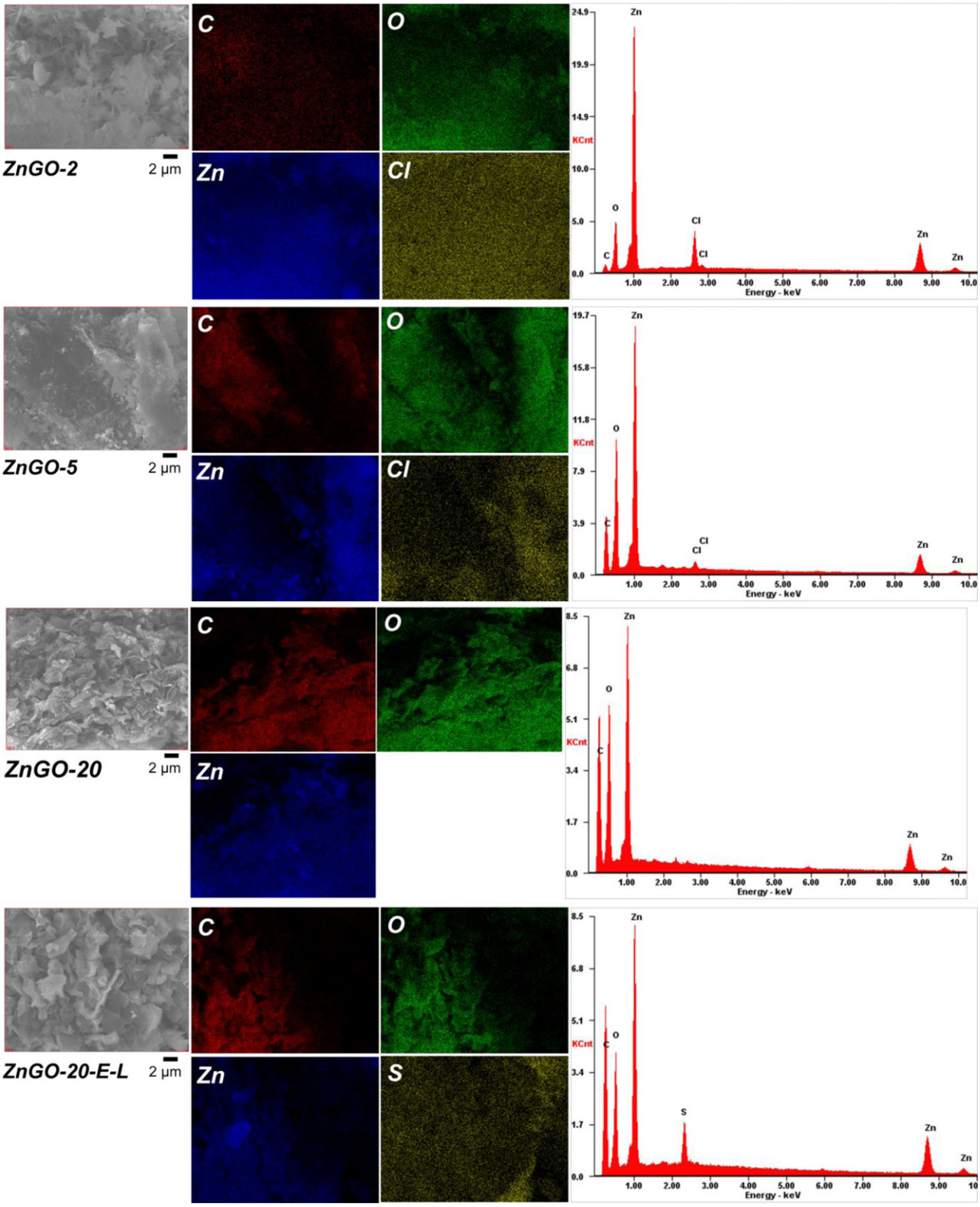

Fig. 2. EDX map of elements for the initial and exhausted samples.

ratio. It is 2.23, 1.02, and 0.5 for ZnGO-2, ZnGO-5 and ZnGO-20, respectively. Even though the GO phase can contribute to the oxygen content, these results suggest that the graphene phase reduces the zinc (hydr)oxide during the composite formation and/or Cl^- replaces the —OH groups.

The texture of our materials should also play a role in their activity for desulfurization. As seen from TEM images presented in Fig. 3, in the case of ZnGO-2 the inorganic phase is evenly distributed on the surface. For the zinc (hydr)oxychloride phase the sizes of the particles calculated from X-ray diffraction pattern

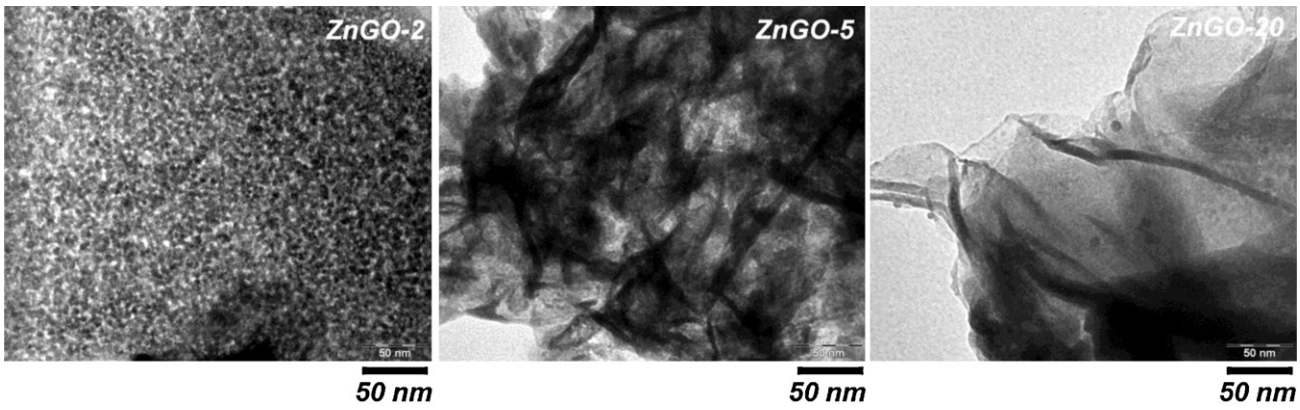

Fig. 3. TEM images for the materials studied.

Table 2
H_2S breakthrough capacities, amount of water preadsorbed, SO_2 released and the surface pH for the materials studied.

Sample	H_2S breakthrough capacity		H_2O adsorbed	Outlet SO_2 concentration	pH	
	(mg/g)	(mg/cm^3)	(mg/g)	(ppm)	In	Exh
ZnGO-2	40	6.8	34	0	6.65	6.65
ZnGO-5	94	16.9	27	0	6.69	6.67
ZnGO-20-E-L	115	43.3	20	0.2	6.57	6.50
ZnGO-20-E-D	155	58.4	24	0.0	6.57	6.49

using Scherrer equation are 20.3 nm. In the case of ZnGO-5 and ZnGO-20 more GO in the samples' composition is clearly seen as flakes. On the surfaces of these flakes the inorganic particles are visible. The size of the particles in the case ZnGO-5 are 17.2 and 21.7 nm for $Zn_5(OH)_8Cl_2{\cdot}nH_2O$ and $ZnO/Zn(OH)_2$, respectively. For the composite with high amount of GO (ZnGO-20) a lack of crystallographic phase of $ZnO/Zn(OH)_2$ is observed. The particles sizes and the degree of surface heterogeneity might also affect the band gap [27–29]. In order for photocatalysis to proceed, the semiconductor needs to absorb energy equal to or more than its energy gap. It is well known that decreasing of the band gap energy can increase the efficiency of the photocatalytic process. Even though the band gap for ZnGO-20 is not known and difficult to measure using optical methods, our recent results indicate a decrease in the energy gap for zinc (hydr)oxide/GO composites with an increase in the GO content. Thus the values found for $Zn(OH)_2$, ZnGO-2 and ZnGO-5 are 3.00, 2.94 and 2.90 eV [30]. This trend suggests that a further decrease in the energy gap for ZnGO-20 can occur and it might reflect in the extent of its photoactivity.

All materials have the surface pH values (Table 2) much smaller than those reported previously (pH 7.3) [9]. This might be related to different batch of GO used to build the composites (more oxidized GO with lower pH in the case of the composites addressed in this paper) and/or to the presence of an inorganic phase, which differs in its chemical nature. Potentiometric titration results further support the differences in the surface chemistry between the composites (Fig. 4). The areas under the peaks at pK_a about 7 represent the absolute numbers of bridging —OH groups and those at pK_a between 10- and 11-terminal —OH groups. As expected based on the GO contents, ZnGO-2 has the highest number of bridging groups. The second peak is shifted to higher pK_a and we linked it to the chemistry associated with the presence of the chloride-containing species. Both ZnGO-5 and ZnGO-20 have similar numbers of terminal groups but less bridging groups are detected in the latter sample. The ratio of terminal to bridging groups should reflect the reactivity of the materials if we assume that the former ones are the centers for H_2S adsorption. The values of 0.38, 0.32, 0.28 and 0.36 for $Zn(OH)_2$, ZnGO-2, ZnGO-5 and ZnGO-20, respectively support

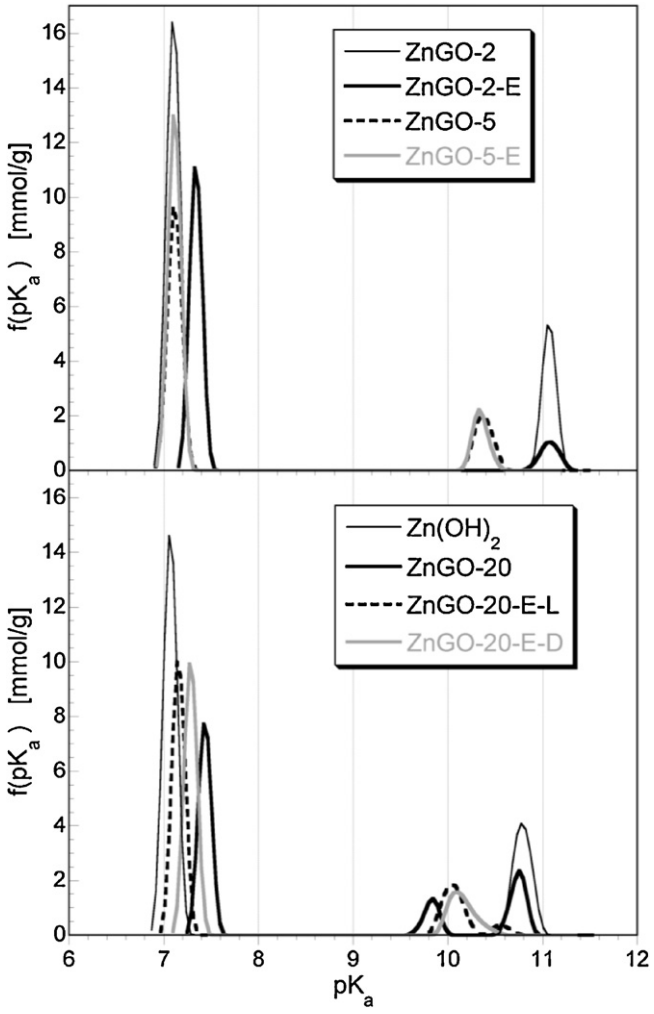

Fig. 4. pK_a distributions for the initial and exhausted composites.

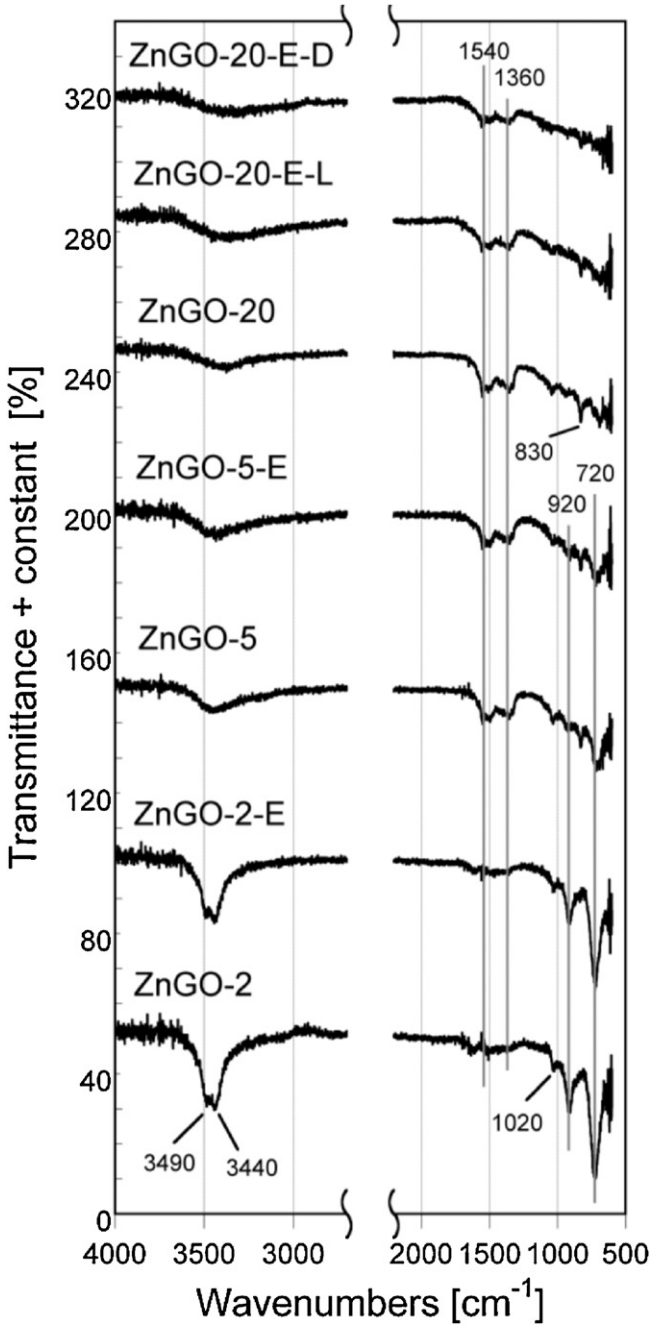

Fig. 5. FTIR spectra for the initial and exhausted materials.

the best performance of the latter sample among the composites. Also on the surface of ZnGO-20 there is a unique peak at pK_a about 9.8 associated with the new chemistry on the interface [9,31]. The comparison of the pK_a distributions for the composites and that for zinc (hydr)oxide reveals the much higher contribution of bridging hydroxyl for the latter material.

The FTIR spectra for the zinc (hydr)oxide composites with GO are presented in Fig. 5. As discussed elsewhere [9,31–33], the broad and intense band around 3500 cm^{-1} is attributed to the fundamental hydroxyl stretching mode of the molecules in the unit cell. They are noticeably more intense in the whole range for the composites with lower contents of GO than those for the ZnGO-20 sample, which is in agreement with the EDX results. There is also a very noticeable splitting of the peak around 3500 cm^{-1} for ZnGO-2. This splitting has been hypothesized to be caused by the intermolecular

Table 3
Parameters of the pore structure calculated from nitrogen adsorption isotherms.

Sample	S_{BET} (m^2/g)	V_t (cm^3/g)	V_{meso} (cm^3/g)	V_{mic} (cm^3/g)	V_{mic}/V_t
ZnGO-2	64	0.086	0.0485	0.038	0.44
ZnGO-5	64	0.375	0.344	0.031	0.08
ZnGO-20	47	0.440	0.418	0.022	0.05

coupling of the OH groups present in both $Zn(OH)_2$ and Zn(OH)Cl of $Zn_5(OH)_8Cl_2$ [32]. All other peaks between 700 and 1600 cm^{-1} originate from various —OH group vibrations [32,34]. The bands at 830 and 1020 cm^{-1} are attributed to the deformation vibration of the OH groups of $Zn(OH)_2$, Zn—OH bending and OH twisting vibrations, while the bands at 720 and 920 cm^{-1} are assigned to the out-of-plane bending mode in Zn(OH)Cl [32]. These bands became less intense with an increase in the graphite oxide content. The two peaks observed at 1360 and 1540 cm^{-1} (with a splitting at 1560 cm^{-1}) are assigned to deformation vibrations of O—H bonds in zinc hydroxide and they are less intense for the ZnGO-2 sample [32]. These peaks can also represent stable forms of chemisorbed oxygen [35] or the stretching modes of zinc acetate-like species shown to be present on this composite when carboxylate groups are available i.e. when the material is sufficiently oxidized [26]. The FTIR analysis confirms the fact that some of the OH groups of the inorganic phase were involved in the composite formation with GO and that the increase in the content of the graphene phase visibly changes the chemistry of the inorganic phase.

Another factor, which differentiates the adsorbents studied is their porosity. The parameters of the porous structure calculated from the nitrogen adsorption isotherms are collected in Table 3. The surface area decreases with an addition of GO and so does the volume of micropores. Interestingly, ZnGO-2 is the most microporous and the ZnGO-5 and ZnGO-20 have a significant volume of large mesopores. We link it to the porosity formed between the flakes of GO with the deposited zinc hydroxide phase. That interface should be much more developed in the composite with the high content of GO. The smaller total volume of pores in this composite compared to that addressed in Ref. [9] (0.561 cm^3/g) can be explained by the presence of highly oxidized and therefore smaller and defected particles GO used. The space between them should be smaller than that when the particles are bigger.

The DTG curves for all initial materials are presented in Fig. 6. The peaks below 100 °C are assigned to the removal of physically adsorbed water and the peaks in the temperature range between 100 and 250 °C represent the removal of water of hydration. Finally,

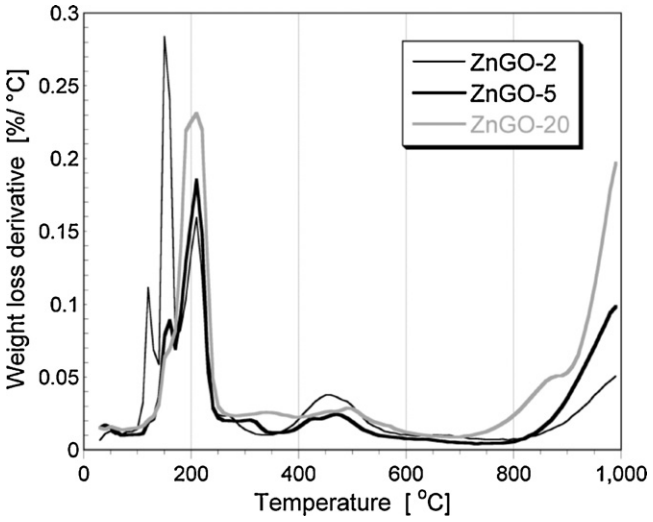

Fig. 6. Comparison of DTG curves in nitrogen for the initial samples.

the peaks between 400 and 600 °C are assigned to the dehydroxylation of the $Zn(OH)_2$ [36]. Another pattern common for all samples is the offset of the huge peak, which starts around 800 °C. This pattern can represent the reduction of GO and/or reduction of zinc oxide by the carbonaceous phase [9,31]. The intensity of this peak decreases with a decrease in the content of graphite oxide. The DTG curves for ZnGO-2 and ZnGO-5 show similar patterns and the differences between the samples are seen only in the intensities of the peaks representing the removal of water of hydration and in the extent of dehydroxylation. Since these peaks are smaller for ZnGO-5 than for ZnGO-2, the addition of slightly more GO apparently caused the formation of a more reduced inorganic phase with less —OH groups being able to retain water. This is consistent with the differences in the water affinity for ZnGO-2 and ZnGO-5 presented in Table 2 and with the XRD and EDX results. In the case of ZnGO-20 the peaks representing the removal of water of hydration/epoxy groups have low intensities and continuous weight losses are noticed between 250 and 700 °C indicating the high degree of chemical heterogeneity. It might be linked to the formation of the new chemistry on the interface between GO and zinc (hydr)oxide. A new intense peak representing decomposition of thermally stable species on the surface of the ZnGO-20 composite appears at about 850 °C. These species might be those new formed on the interface between GO and the inorganic phase.

3.2. Performance of the composites as H_2S adsorbents

The measured breakthrough curves on the composites studied are collected in Fig. 7. The steep desorption curves indicate the strong adsorption of H_2S. For all samples except for ZnGO-20 SO_2 was not detected in the outlet gas during the duration of the experiments. This suggests that the ability of the materials to oxidize H_2S to SO_2 decreases with a decrease in the content of graphite oxide. Alternatively, it could also signify that the materials with smaller amounts of GO have a better ability to adsorb SO_2 formed on the surface. H_2S breakthrough experiments were only carried out in moist air. As reported previously [9–11,37], the high adsorption capacities in moist conditions are linked to the extent of the dissociation of H_2S to HS^-. It is a critical step in the adsorption of hydrogen sulfide on metal oxides and carbonaceous materials [38]. This dissociation process governed by the surface chemical nature/pH also facilitates the acid–base reactions.

The ZnGO-20 sample, owing to its good performance in ambient light, was chosen to run experiments in dark. As seen in Fig. 7, the lack of light significantly increases the capacity for H_2S removal. This result does not cross out the hypothesis formulated elsewhere [9] that visible light enhances the oxidation of H_2S to SO_2 on zinc (hydr)oxide/GO composites. That oxidation might be beneficial for the performance of the composite in comparison with zinc (hydr)oxide but apparently it does not increase the efficiency of desulfurization on the composite itself.

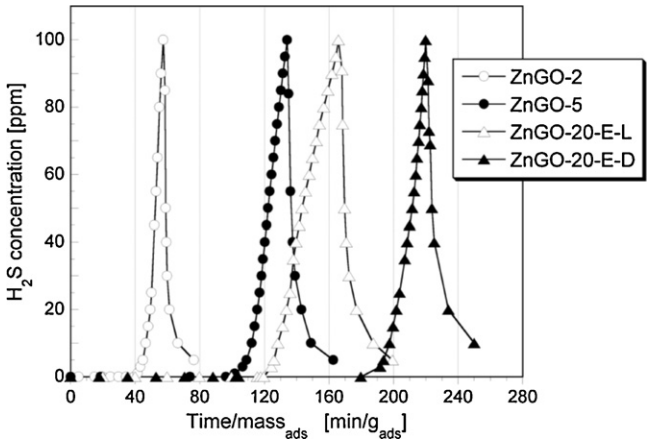

Fig. 7. H_2S breakthrough curves measured in moist conditions on the materials studied.

The calculated breakthrough capacities, the amount of water preadsorbed during prehumidification, and the surface pH values are collected in Table 2. The ability of the composites to adsorb hydrogen sulfide differs and the capacities range from 40 mg/g on ZnGO-2 to 155 mg/g on ZnGO-20. The latter is measured in dark conditions. Interestingly, on the material with 20 wt.% GO the smaller adsorption capacity than that reported previously on the sample of similar composition (155 mg/g vs 211 mg/g [9]) is found. The ability to adsorb water also differs for the various zinc (hydr)oxide/graphite oxide composites. Though the shapes of the breakthrough curves are similar for all composites, the slopes are less steep for the materials exhibiting the higher adsorption capacities.

3.3. Analysis of the exhausted samples

To derive the mechanism of reactive adsorption and to evaluate the effects of the light exposure, the exhausted materials have to be extensively characterized and the results of these analyses should be compared to those obtained on the initial samples [39]. A general trend in the results obtained is an increase in the amount of H_2S adsorbed with an increase in the amount of GO in the composites with zinc (hydr)oxide. This is opposite to the trend found on the cobalt hydroxide/graphite oxide materials where the smaller mass ratio of graphite oxide resulted in the better adsorption capacities [10]. These results indicate a difference between the adsorption mechanism of hydrogen sulfide on zinc (hydr)oxide/graphite oxide based materials and that on the cobalt hydroxide/graphite oxide composites.

For all exhausted samples the XRD patterns (Fig. 1) reveal peaks representing the crystallographic phases of zinc sulfide at 28.36°, 47.40°, 50.05°, 56.64° and 58.42° [40] and zinc sulfite at 11.43° and 32.62° [41]. The peaks associated to the $Zn_5(OH)_8Cl_2{\cdot}nH_2O$ phase in the initial samples with 2 and 5% GO are replaced by peaks characteristic to zinc sulfite (as seen by slightly shift of the peak at 11.43°) and $ZnO/Zn(OH)_2$. They are likely a result of the reaction of H_2S with the surface active sites in the presence of water. Apparently after running experiments in dark on ZnGO-20 the ZnS crystalline phase is much more pronounced than that formed in light, which supports our hypothesis about the influence of visible light on the oxidation of hydrogen sulfide [9].

After exposure to hydrogen sulfide in ambient light that ratio of Zn/O for ZnGO-20-E-L increased more than three times to 1.78 and 6.7 at.% sulfur is present on the surface. The HS^- groups likely replaced the —OH groups and/or elemental sulfur is deposited on the surface. Nevertheless, when taking that replacement into account and assuming that all sulfur is present as sulfides, the decrease in the oxygen content is significant. This might be the result of the reduction of GO and $Zn(OH)_2$ by electrons as a result of photoactivity of the composite in visible light and water splitting reaction [9,42]. As discussed above, the GO used to form this particular composite was on higher oxidation state than that used to build the composite addressed in Ref. [9].

Exposure of the composite samples to H_2S in pre-humidified moist conditions results in the changes in surface chemistry seen on the DTG curves (Fig. 8). For the ZnGO-2 sample there is an increase in the intensity of the peaks assigned to the removal of water of hydration centered at 160 °C and an increase in the intensity of the peaks between 400 and 600 °C. The latter peaks may be linked to the effect of the decomposition of zinc sulfite/sulfate [43] combined with the dehydroxylation of zinc hydroxide expected at the

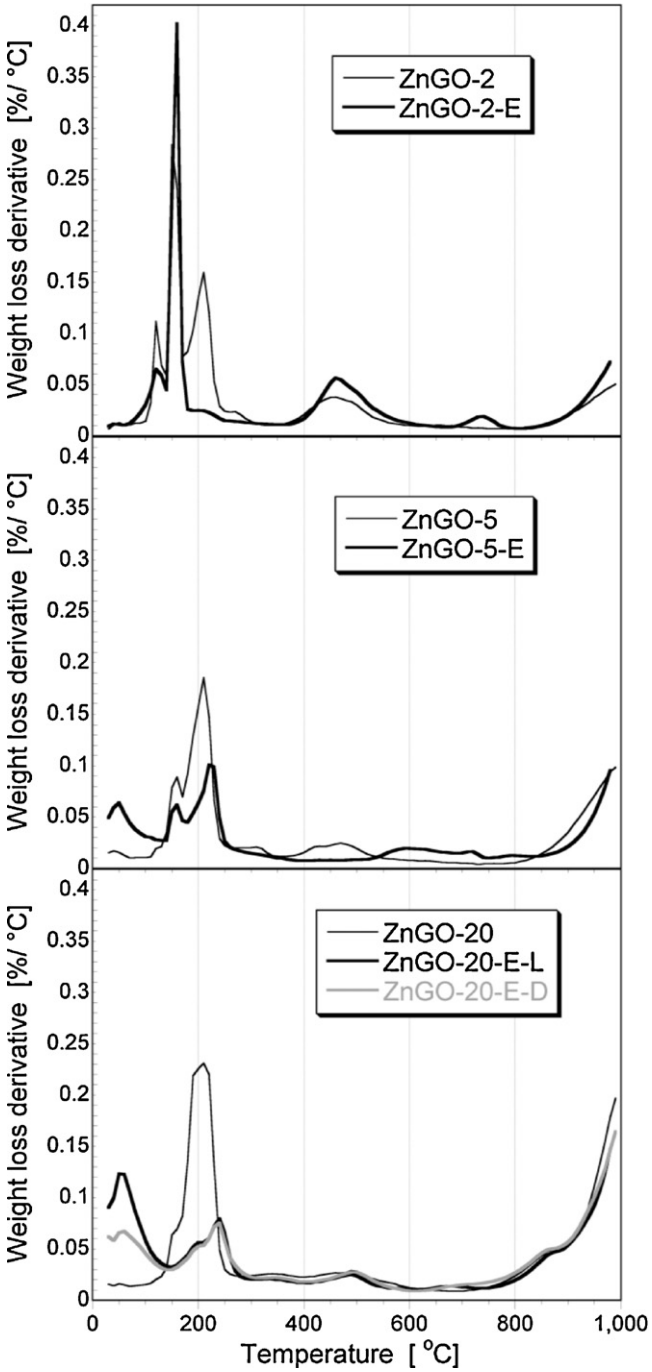

Fig. 8. DTG curves in nitrogen for the initial and exhausted composites.

same temperature range. A new peak appears at about 770 °C and we link it to the decomposition of $ZnSO_4$ [44]. The opposite effects are found for the ZnGO-5 and ZnGO-20 samples where the peaks corresponding to the dehydroxylation and to the removal of water of hydration decrease in their intensity. This decrease suggests the interactions of hydroxyl groups with H_2S and sulfidation of the surface. These new species are removed in a broad temperature range between 500 and 800 °C. An increase in the intensity of the peak at the temperature less than 100 °C is noticed for the best adsorbents, ZnGO-5 and ZnGO-20. This can be explained by the removal of physically adsorbed H_2S and SO_2. ZnGO-20-E-L exhibits a significant decrease in the amount of water of hydration, which is linked to the replacement of OH groups with more hydrophobic sulfur. Moreover, water splitting in visible light [9,42] can also contribute to this decrease. Interestingly, no differences between the initial and exhausted samples are noticed at the higher temperature range. The DTG curve for the sample run in dark exhibits a lower intensity of the peak at about 100 °C compared to that for ZnGO-20-E-L. Since it happens in spite of the fact that the experiment in dark was run longer time and more water could be adsorbed, we link this peak to weakly adsorbed SO_2. More of this species is formed when the sample was exposed to visible light.

The consumption of terminal groups after H_2S adsorption is also clearly seen from the results of potentiometric titration when the initial and exhausted samples are compared (Fig. 4). Moreover, the involvement of these OH centers in the case of ZnGO-20 is much more visible for the breakthrough experiment run in dark than that in ambient light. This suggests that light suppresses the direct acid–base reaction of hydrogen sulfide with the surface of zinc (hydr)oxide.

After exposure to H_2S the intensity of almost all bands of the IR spectra noticeably decreased for all samples (Fig. 5). Since the majority of vibrations represent OH groups, the decrease in their intensity is linked to the involvement of these groups in the H_2S reactive adsorption. This is in agreement with the thermogravimetric analysis, potentiometric titration, and EDX results discussed above. A similar trend was observed on the cobalt hydroxide/GO composites and the decrease in the bands' intensity was linked to the formation of sulfides. The comparison of the spectra for ZnGO run in dark and in ambient light shows that the decrease in the intensity of the OH band is more pronounced in dark, which we link to the higher capacity and more sulfides formed on the surface. Moreover, a decrease in the intensity of the bands linked to GO chemistry [45] is noticed for the sample run in dark. This might be the result of the reducing effect of hydrogen sulfide.

The differences mentioned above in the chemistry and texture are also seen on H_2S adsorption heat flow curves for the materials exposed to dry H_2S in air or in nitrogen (Fig. 9). Various peaks/shoulders are exhibited on the curves related to surface heterogeneity and the presence of adsorption centers. The first peak represents the highest energy centers. Its broadness is related to the amount of these centers and thus to the amount of H_2S adsorbed. We cannot normalize the results per the amount of H_2S adsorbed since our breakthrough experiments were run in moist conditions. Nevertheless, a similar order in the performance in dry conditions is expected as that presented in Table 2 [9]. A very steep increase in the heat upon exposure to H_2S is found for the composites with 2 and 5% of GO and the effect for the latter sample is much more intense. The curve for ZnGO-20 resembles that for $Zn(OH)_2$ with similar ratio of the intensities of the two peaks. Nevertheless, the composites have more high-energy centers. Low energy centers are seen on $Zn(OH)_2$ as a broad tail with the progress of adsorption. The ratio of the peak intensity related to the highest energy centers to that represented by the shoulder is the greatest for ZnGO-2 and decreases with an increase in the GO content. Based on the results of structural and chemical analyses presented above we link the heat effect represented by the first peaks of ZnGO-2 to the replacement of Cl^- ions by HS^- ions in its composition with zinc (hydr)oxychlorides. The presence of micropores in this material should also play a role in the H_2S attraction. Then the intensity of the peak increases for ZnGO-5 since still Cl is present here. Even though the quantity of Cl is smaller than that in ZnGO-2, the terminal hydroxyls may compensate this effect. For ZnGO-20, only the interactions with the surface hydroxyls are represented by that peak. Running experiments in air must cause the oxidation of some hydrogen sulfide by active oxygen and the second peak/shoulder might be linked to this process. The relatively high intensities of the second peak compared to the first for ZnGO-2 might represent reaction of SO_2 with the terminal OH groups [15,42].

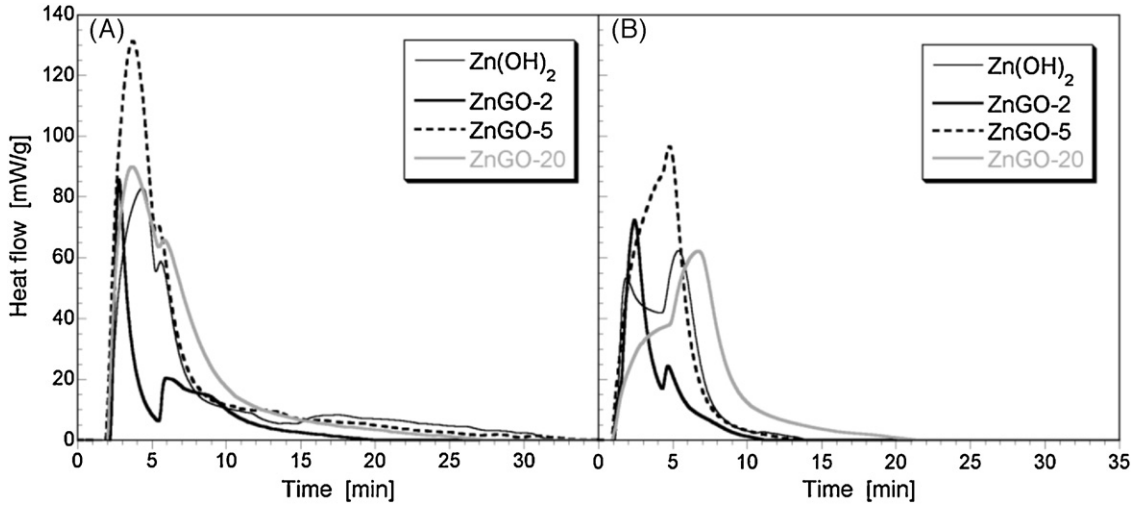

Fig. 9. Heat flow curves for H_2S adsorption on the materials studied in air (A) and in nitrogen (B).

3.4. Proposing the mechanism of H_2S reactive adsorption

Since the H_2S removal capacity on zinc (hydr)oxide reported previously was 139 mg/g in moist conditions in ambient light [9] the synergistic effect in the case of the materials studied here is found only for the composite with 20 wt.% of GO. This suggests that the content of GO in the composite affects the chemistry of the composite and it is important to stimulate the surface reactions. The

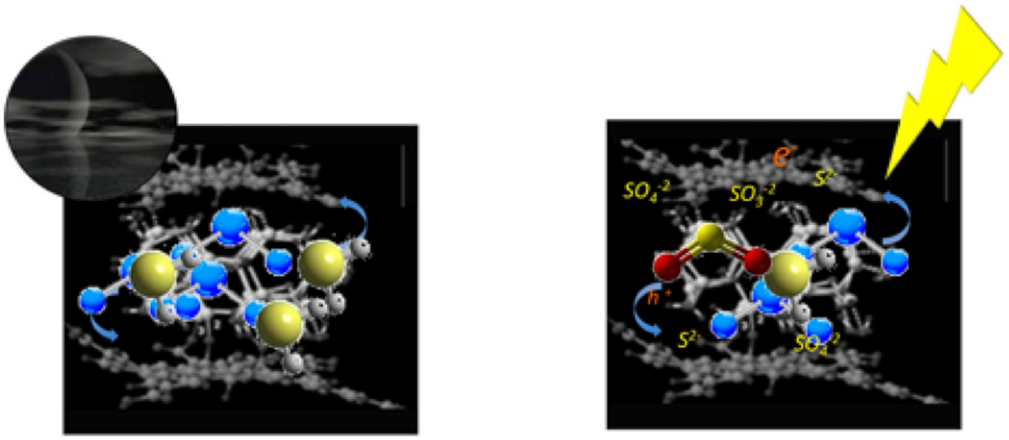

$$H_2O + H_2S \longrightarrow HS^- + H_3O^+$$
$$Zn\text{-}OH + HS^- \longrightarrow Zn\text{-}HS + OH^-$$

$$ZnOH\text{-}GO + h\nu \longrightarrow e^-(GO) + h^+(Zn\text{-}OH)$$
$$e^- + O_2 \longrightarrow O_2^{\bullet -}$$
$$h^+ + OH^- \longrightarrow OH^\bullet$$
$$O_2^{\bullet -} + H_2O \longrightarrow OH_2^\bullet + OH^-$$
$$OH_2^\bullet + H_2O \longrightarrow H_2O_2 + OH^\bullet$$
$$H_2O_2 \longrightarrow 2OH^\bullet$$

$$H_2O + H_2S \longrightarrow HS^- + H_3O^+$$
$$Zn\text{-}OH + HS^- \longrightarrow Zn\text{-}HS + OH^-$$

$$HS^- + OH^\bullet \longrightarrow S^0 + H_2O$$
$$HS^- + OH^\bullet + H_2O \longrightarrow HSO_3^\bullet + H^+$$
$$Zn\text{-}OH + HSO_3^- \longrightarrow Zn\text{-}HSO_3^\bullet + OH^-$$

Fig. 10. Proposed mechanisms of H_2S reactive adsorption in dark and in light.

capacity of ZnGO-20 in dark is about 50% higher than that in light. When the SO_2 capacity of this sample was analyzed in ambient light and dark, exposure to light resulted in a significant increase in the capacity with a marked amount of H_2S released from the surface [42]. It was linked to the effect of light on water splitting and the participation of water in reduction of SO_2 to sulfides. In the case of hydrogen sulfide adsorption water splitting, even if it happens in light, cannot further reduce sulfur species. On the other hand, light can participate in formation of holes and electrons. While the former form OH• radicals in reactions with OH-groups, the latter leads to active oxygen ions which a further contribute to the formation of OH• radicals in their reactions with water [18]. These species oxidize hydrogen sulfide to elemental sulfur or SO_2 and thus sulfites are detected on the surface. The deposition of that sulfur can block the active centers and terminal OH groups for the reaction with hydrogen sulfide. The much higher H_2S removal capacity in dark than that in light is linked to more OH^- groups available for reactions with HS^- since these groups are not involved in the formation of radicals. It might also happen that it light-generated electrons are able to reduce the highly oxidized GO phase and thus they limit the participation of its oxygen groups in the formation of superoxygen ions [46,47]. The reducing effect caused by electrons can also affect the chemistry of the zinc based inorganic phase resulting in less —OH group for interactions with H_2S. Taking into account all the above considerations the mechanisms of H_2S reactive adsorption on the ZnGO-20 in dark and under ambient light exposure are presented in Fig. 10.

To explain the difference between the performance of ZnGO-20 and that composite reported in Ref. [9] much smaller surface pH of our materials that than those reported previously (pH 7.3) should be taken into consideration. As mentioned above, this is the result of the different batch of GO used to build the composites (more oxidized GO, pH 1.90) and/or to the presence of the inorganic phase that differs in its chemical nature. This low pH can be responsible for the smaller adsorption capacity on these materials since it is known that basic pH promotes H_2S removal [4,7,37,48]. For the composite with the highest capacity, the pH slightly decreases after adsorption, which is an indication of the consumption of some basic groups and/or formation of acidic species on the surface. This material also has the lowest initial pH indicating that the GO amount governs the chemistry of the composite.

Apparently, the composites with a higher contribution of large pores are better adsorbents of hydrogen sulfide. These mesopores might be the transport pores providing water for the specific nanoreactor small pores on the interface of GO and the zinc (hydr)oxide phase where the surface synergy of the composite plays the most important role.

3.5. Heat of H_2S interactions with the surface of the composites

When the heat of adsorption was measured in the absence of oxygen different patterns were revealed than those in air. Interestingly, the curves for ZnGO-2 in air and nitrogen resemble each other, which suggest that oxidation of H_2S is not a significant mechanism of H_2S removal on this material and the replacement reactions and physical adsorption are important interaction paths. This behavior might be linked to the small amount of graphene and the presence of a zinc hydr(oxy)chloride phase. The curve for $Zn(OH)_2$ reveals two peaks, which we link to the interactions of H_2S with the terminal and bridging hydroxyls. The heats value obtained after deconvolution of heat flow curves are summarized in Table 4. The total heat values in air are about 10 J/g greater than those in nitrogen. Much higher heats in air than in nitrogen for all samples but ZnGO-2 indicate that oxidation is an important energetic effect. While that increase in air is 49, 40, and 40% for $Zn(OH)_2$, ZnGO-5 and ZnGO-20, respectively, it is only 30% (about 3 J/g) for ZnGO-2.

Table 4
Heat of H_2S adsorption on the materials studied in different conditions.

Sample	Peak 1	Peak 2	Peak 3
Heat of H_2S adsorption in nitrogen [J/g]			
$Zn(OH)_2$	3.60	9.67	4.46
ZnGO-2	6.43	4.01	
ZnGO-5	16.97	5.99	
ZnGO-20	14.94	6.48	
Heat of H_2S adsorption in air [J/g]			
$Zn(OH)_2$	19.22	7.30	
ZnGO-2	5.65	3.79	4.17
ZnGO-5	27.78	5.66	
ZnGO-20	29.77	1.29	

This once again is linked to the differences in the chemistry and in the numbers of OH groups in the inorganic phase. The heat effect represented by the first peak is much greater for the composites than for the zinc (hydr)oxide. This supports the hypothesis about the importance of GO for the development of high energetic sites and for the extent of the H_2S adsorption/oxidation process.

4. Conclusions

The specific surface features of the zinc (hydr)oxide/graphene oxide and zinc (hydr)oxychlorides/graphene oxides composites govern their performance as adsorbents of hydrogen sulfide. The composites with 2 and 5 wt.% graphite oxide have smaller adsorption capacities because zinc (hydr)oxychloride is present in their chemical composition. The new batch of composites with 20 wt.% graphite oxide also exhibits a smaller adsorption capacity than the zinc (hydr)oxide/graphite oxide composite reported earlier. This is as a result of a more oxidized form of graphite oxide used as a composite component, which leads to the acidic surface pH suppressing H_2S dissociation. The visible light activity of the composite causes the reduction of that highly oxidized GO surface and thus restricts its ability to activate oxygen. Moreover, the involvement of OH groups in the formation of radicals, oxidation of H_2S to elemental sulfur and its deposition on the surface limit the numbers of the OH group for the surface reactions with H_2S. In dark the oxidation of H_2S is limited and the terminal groups play an important role in the removal process.

Acknowledgements

This work was supported by ARO Grant W911NF-10-1-0039, NSF collaborative grant CBET 1133112.

References

[1] W. Feng, S. Kwon, E. Borguet, R. Vidic, Environmental Science and Technology 39 (2005) 9744–9749.
[2] G.A. Bukhtiyarova, I.V. Delii, N.S. Sakaeva, V.V. Kaichev, L.M. Plyasova, V.I. Bukhtiyarov, Reaction Kinetics and Catalysis Letters 92 (2007) 89–97.
[3] H.F. Garces, H.M. Galindo, L.J. Garces, J. Hunt, A. Morey, S.L. Suib, Microporous and Mesoporous Materials 127 (2010) 190–197.
[4] A. Bagreev, J.A. Menendez, I. Dukhno, Y. Tarasenko, T.J. Bandosz, Carbon 42 (2004) 469–476.
[5] A. Bagreev, T.J. Bandosz, Industrial and Engineering Chemistry Research 41 (2002) 672–679.
[6] J. Przepiorski, A. Oya, Journal of Materials Science Letters 17 (1998) 679–682.
[7] M. Seredych, T.J. Bandosz, Materials Chemistry and Physics 113 (2009) 946–952.
[8] S. Bashkova, F.S. Baker, X. Wu, T.R. Armstrong, V. Schwartz, Carbon 45 (2007) 1354–1363.
[9] M. Seredych, O. Mabayoje, T.J. Bandosz, Langmuir 28 (2011) 1337–1346.
[10] O. Mabayoje, M. Seredych, T.J. Bandosz, Journal of Colloid and Interface Science 378 (2012) 1–9.
[11] M. Seredych, T.J. Bandosz, Chemical Engineering Journal 166 (2011) 1032–1038.
[12] L.B. Casabianca, M.A. Shaibat, W.W. Cai, S. Park, R. Piner, R.S. Ruoff, Y. Ishii, Journal of the American Chemical Society 132 (2010) 5672–5676.
[13] T. Szabo, O. Berkesi, P. Forgo, K. Josepovits, Y. Sanakis, D. Petridis, I. Dekany, Chemistry of Materials 18 (2006) 2740–2749.

[14] D.R. Dreyer, S. Park, C.W. Bielawski, R.S. Ruoff, Chemical Society Reviews 39 (2010) 228–240.
[15] M. Seredych, T.J. Bandosz, Journal of Physical Chemistry C 114 (2010) 14552–14560.
[16] M.Y. Guo, A.M.C. Ng, F. Liu, A.B. Djurisic, W.K. Chan, Applied Catalysis B: Environmental 107 (2011) 150–157.
[17] H. Qin, W. Li, Y. Xia, T. He, ACS Applied Materials and Interfaces 3 (2011) 3152–3156.
[18] J. Mu, C. Shao, Z. Guo, Z. Zhang, M. Zhang, P. Zhang, B. Chen, Y. Liu, ACS Applied Materials and Interfaces 3 (2011) 590–596.
[19] W.S. Hummers, R.E. Offeman, Journal of the American Chemical Society 80 (1958) 1339.
[20] M.M. Dubinin, in: P.L. Walker (Ed.), Chemistry and Physics of Carbon, vol. 2, Marcel Dekker, New York, USA, 1966, pp. 51–120.
[21] J. Jagiello, Langmuir 10 (1994) 2778–2785.
[22] J. Jagiello, T.J. Bandosz, J.A. Schwarz, Carbon 32 (1994) 1026–1028.
[23] A. Bagreev, H. Rahman, T.J. Bandosz, Carbon 39 (2001) 1319–1326.
[24] H. Tanaka, A. Fujioka, A. Futoyu, K. Kandori, T. Ishikawa, Journal of Solid State Chemistry 180 (2007) 2061–2066.
[25] A.P.A. Oliveira, J.-F. Hochepied, F. Grillon, M.-H. Berger, Chemistry of Materials 15 (2003) 3202–3207.
[26] S. Inoue, S. Fujihara, Inorganic Chemistry 50 (2011) 3605–3612.
[27] M. Kranjcec, I.P. Studenyak, M.V. Kuric, Journal of Non-crystalline Solids 355 (2009) 54–57.
[28] X. Chen, L. Liu, P.Y. Yu, S.S. Mao, Science 331 (2011) 746–750.
[29] A.A. Dakhel, Optical Materials 31 (2009) 691–695.
[30] S.M.Z. Islam, T. Gayen, M. Seredych, O. Mabayoye, T.J. Bandosz, R. Alfano, Optics Communications (submitted).
[31] M. Seredych, O. Mabayoje, M.M. Koleśnik, V. Krstić, T.J. Bandosz, Journal of Materials Chemistry 22 (2012) 7970–7978.
[32] O.K. Srivastava, E.A. Secco, Canadian Journal of Chemistry 45 (1967) 585–588.
[33] A.A. Tsyganenko, V.N. Filimonov, Journal of Molecular Structure 19 (1973) 579–589.
[34] B.M. Keyes, L.M. Gedvilas, X. Li, T.J. Coutts, Journal of Crystal Growth 281 (2005) 297–302.
[35] J. Zawadzki, in: P.A. Thrower (Ed.), Chemistry and Physics of Carbon, vol. 21, Dekker, New York, 1989, pp. 180–200.
[36] C. Woll, Progress in Surface Science 82 (2007) 55–120.
[37] T.J. Bandosz, Journal of Colloid and Interface Science 246 (2002) 1–20.
[38] T.J. Bandosz, in: T.J. Bandosz (Ed.), Activated Carbon Surfaces in Environmental Remediation, vol. 7, Elsevier, Amsterdam, 2006, pp. 231–292.
[39] T.J. Bandosz, Catalysis Today 186 (2012) 20–28.
[40] A. Samokhvalov, B.J. Tatarchuk, Physical Chemistry Chemical Physics 13 (2011) 3197–3209.
[41] V.D. Khavryuchenko, O.V. Khavryuchenko, V.V. Lisnyak, Catalysis Communications 11 (2010) 340–345.
[42] M. Seredych, O. Mabayoje, T.J. Bandosz, Applied Catalysis B: Environmental, http://dx.doi.org/10.1016/j.apcatb.2012.12.011 (in press).
[43] R.C. Weast, M.J. Astle (Eds.), Handbook of Chemistry and Physics, 62nd ed., CRC Press, Boca Raton, FL, USA, 1981, p. B-165.
[44] R.V. Siriwardane, J.A. Poston Jr., E.P. Fisher, M.-S. Shen, A.L. Miltz, Applied Surface Science 152 (1999) 219–236.
[45] M. Seredych, J.A. Rossin, T.J. Bandosz, Carbon 49 (2011) 4392–4402.
[46] B. Stohr, H.P. Boehm, Carbon 29 (1991) 707–720.
[47] V.V. Strelko, N.T. Kartel, I.N. Dukhno, V.S. Kuts, R.B. Clarkson, B.M. Odintsov, Surface Science 548 (2004) 281–290.
[48] F. Adib, A. Bagreev, T.J. Bandosz, Journal of Colloid and Interface Science 216 (1999) 360–369.